CONDENSED MATTER PHYSICS

Phase engineering of anomalous Josephson effect derived from Andreev molecules

Sadashige Matsuo[1]*, Takaya Imoto[1,2], Tomohiro Yokoyama[3], Yosuke Sato[1], Tyler Lindemann[4,5], Sergei Gronin[4], Geoffrey C. Gardner[4], Michael J. Manfra[4,5,6,7], Seigo Tarucha[1,8]*

A Josephson junction (JJ) is a key device for developing superconducting circuits, wherein a supercurrent in the JJ is controlled by the phase difference between the two superconducting electrodes. When two JJs sharing one superconducting electrode are coherently coupled and form the Andreev molecules, a supercurrent of one JJ is expected to be nonlocally controlled by the phase difference of another JJ. Here, we evaluate the supercurrent in one of the coupled two JJs as a function of local and nonlocal phase differences. Consequently, the results exhibit that the nonlocal phase control generates a finite supercurrent even when the local phase difference is zero. In addition, an offset of the local phase difference giving the JJ ground state depends on the nonlocal phase difference. These features demonstrate the anomalous Josephson effect realized by the nonlocal phase control. Our results provide a useful concept for engineering superconducting devices such as phase batteries and dissipationless rectifiers.

INTRODUCTION

Symmetry-breaking superconducting (SC) junctions have often been used to explore exotic SC phenomena including SC diodes (*1*–*3*), topological superconductivity, and Majorana zero modes (*4*). The Josephson junction (JJ) (*5*) is an SC device that is often used for searching such SC phenomena. The JJs exhibit anomalous Josephson effect (AJE) upon the disorientation of the time-reversal and spatial-inversion symmetries, in which a finite phase difference away from 0 and π produces the ground state of the JJ, called the φ junction (*6*–*14*). Simultaneously, a finite supercurrent is present even at zero phase difference, called the spontaneous supercurrent. The φ junction has recently attracted considerable attention for manifold applications in SC phase batteries (*11*, *15*) and SC diodes (*1*, *16*–*19*). To date, various systems have been proposed for realizing the φ junctions, such as JJs consisting of s-wave SC electrodes and a normal metal holding the spin-orbit interactions in strong magnetic fields (*6*–*10*), and have been experimentally verified as well (*11*–*14*). When the strong magnetic fields or ferromagnetism is committed to disintegrate the time-reversal symmetry, they can degrade the superconductivity. On the other hand, the phase control of the SC devices also breaks the time-reversal symmetry and is available to realize the SC diode effect (*20*–*23*). This implies that the phase control is useful to engineer the AJE in the SC devices.

Recently, it has been proposed that short-range coherent coupling of two JJs sharing one SC electrode can hybridize the Andreev bound states (ABSs) (*24*–*27*) in the respective JJs to form Andreev molecule states (AMSs) (*28*–*34*). The coherent coupling through the shared SC electrode is intermediated by elastic cotunneling or crossed Andreev reflection (*35*–*43*), and the SC transport has been studied theoretically and experimentally (*28*, *44*–*49*). The AMSs in the coupled two JJs generate the nonlocal Josephson effect, where the supercurrent in a JJ depends on the local phase difference as well as the nonlocal phase difference of the other JJ (*28*).

In the coupled JJs illustrated in Fig. 1A, the supercurrent in the JJ1 satisfies the time-reversal relation of $I_{sc1}(\phi_1, \phi_2) = -I_{sc1}(-\phi_1, -\phi_2)$, where ϕ_1 and ϕ_2 denote the phase differences in JJ1 and JJ2, respectively. When the SC phases of the upper, shared, and lower electrodes are defined as θ_u, θ_s,and θ_l respectively, the local and nonlocal phase differences of ϕ_1 and ϕ_2 are given as $\phi_1 = \theta_s - \theta_u$ and $\phi_2 = \theta_l - \theta_s$. Upon setting ϕ_2 and considering only JJ1, a character of the φ junction can emerge (*28*) because the time reversal and spatial inversion symmetries can be regarded as disintegrated at $\phi_2 \neq 0, \pi$. This realization method requires neither strong magnetic fields nor ferromagnetic materials. Furthermore, the φ junction and spontaneous supercurrent of JJ1 obtained by the mechanism are nonlocally controllable through JJ2, which will provide a useful method to control phase batteries or SC diodes. We have previously demonstrated the SC diode effect derived from the coherent coupling, namely, the AMSs (*45*). However, the AJE (spontaneous supercurrent and φ junction) has not yet been experimentally verified.

In this study, we succeed in evaluating the supercurrent in JJ1 as a function of ϕ_1 and ϕ_2. The obtained results exhibit the supercurrent dependent on not only ϕ_1 but also ϕ_2. In the dependence, the spontaneous supercurrent and φ junction derived from the AMSs formed in the coupled two planar JJs are found. It is predicted that although the topological superconductivity is engineered in single planar JJs with the phase control and the Zeeman field (*50*–*52*), the coherent coupling of two planar JJs engineers the topological superconductivity only with the phase control (*53*, *54*). For the realization, it is demanded to elucidate the fundamental physics of the AMSs in the coupled JJs, especially about the symmetry

[1]Center for Emergent Matter Science, RIKEN, Wako, Saitama 351-0198, Japan. [2]Department of Applied Physics, Tokyo University of Science, Shinjuku-ku, Tokyo 162-8601, Japan. [3]Department of Materials Engineering Science, Graduate School of Engineering Science, Osaka University, Toyonaka, Osaka 560-8531, Japan. [4]Birck Nanotechnology Center, Purdue University,, West Lafayette, IN 47907, USA. [5]Department of Physics and Astronomy, Purdue University, West Lafayette, IN 47907, USA. [6]School of Materials Engineering, Purdue University, West Lafayette, IN 47907, USA. [7]Elmore Family School of Electrical and Computer Engineering, Purdue University, West Lafayette, IN 47907, USA. [8]RIKEN Center for Quantum Computing, RIKEN, Wako, Saitama 351-0198, Japan.
*Corresponding author. Email: sadashige.matsuo@riken.jp (S.M.); tarucha@riken.jp (S.T.)

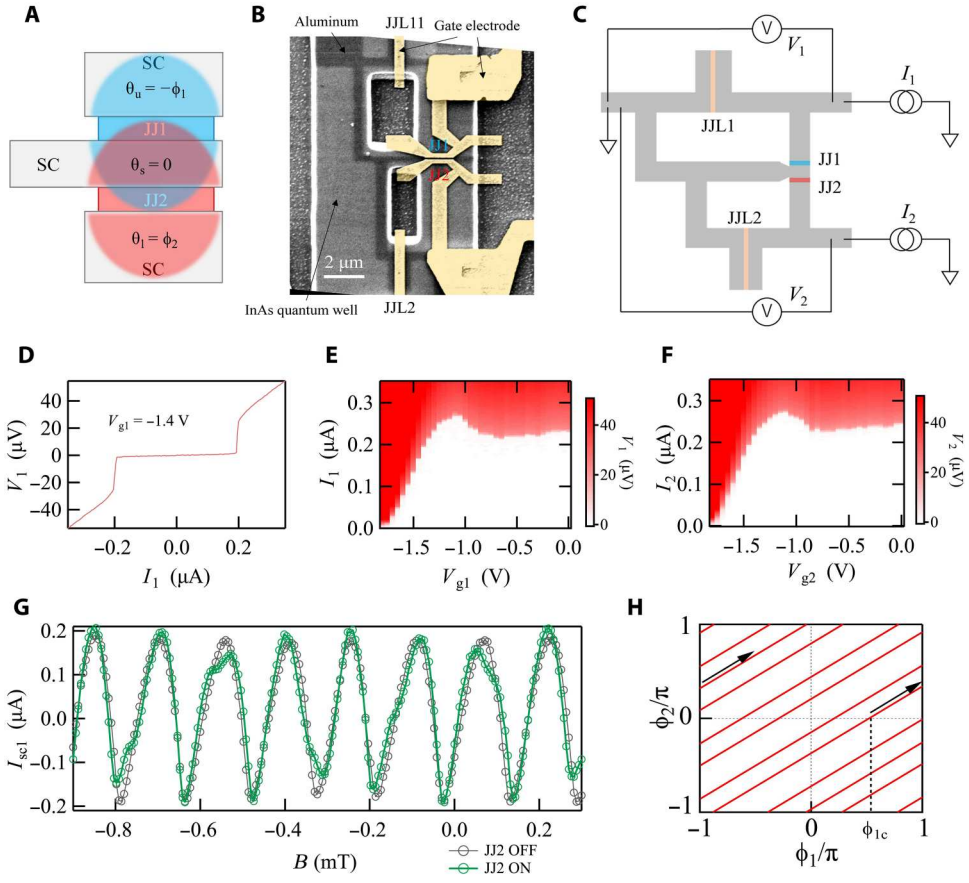

Fig. 1. Concept and device. A conceptual image of coupling between two JJs. Overlapping of wave functions of ABSs in the shared SC electrode connects the two JJs to form AMSs. The SC phases for the respective electrodes are labeled. (**A**) SEM image of our device. The black region represents the aluminum electrodes. The respective JJs are covered by the gate electrodes highlighted in yellow. (**B**) Schematic of our device and measurement circuit. (**C**) Typical *I-V* curve of the single JJ1 at $V_{g1} = -1.4$ V with the other JJs off at $B = 0$ mT. (**D**) V_1 as a function of I_1 and V_{g1} at $B = 0$ mT to characterize the gate dependence of the single JJ1 with the other JJs off. The supercurrent of JJ1 is highly tunable in the V_{g1} range of -1.9 V $< V_{g1} < -1.3$ V. Then, the CPR of JJ1 is studied in this range. (**E**) V_2 as a function of I_2 and V_{g2} at $B = 0$ mT to characterize the gate dependence of the single JJ2. The supercurrent of JJ2 is highly tunable in -2.0 V $< V_{g1} < -1.4$ V. (**F**) The supercurrent in the single JJ1 (the black circles) and the JJ1 coupled to JJ2 (the green circles) as a function of *B* evaluated from the switching current measurement of the larger asymmetric SQUID. The curve in the single JJ1 case periodically oscillates to *B*, while the curve in the coupled JJ1 case is not periodic due to modulation from the coherent coupling. (**G**) The (ϕ_1, ϕ_2) trace as *B* is swept in the case that all the JJs are on. From the measurement of the larger SQUID with $I_2 = 0$ nA, the JJ1 CPR on the trace lines can be obtained.

breaking invoked by the phase control. In this sense, the phase-engineering of the AJE in the planar JJs contributes to realizing the topological superconductivity only by the phase control.

To demonstrate the phase engineering of the AJE, we need to evaluate the two-dimensional current phase relation (CPR) $I_{sc1}(\phi_1, \phi_2)$, i.e., the supercurrent in JJ1, as a function of the local and nonlocal phase differences. For this sake, we use asymmetric SC quantum interference devices (SQUIDs) (*55*) whose scanning electron microscopy (SEM) image and schematic are shown in Fig. 1 (B and C), respectively. The device is fabricated on a high-quality InAs quantum well covered with an epitaxial aluminum thin film. The stacking of the epitaxial aluminum and the InAs quantum well provides a highly transparent interface to provide an ideal platform for studying the physics of superconductor-semiconductor junctions (*56*–*58*). The device includes the coupled JJs (JJ1 and JJ2) with a shared SC electrode 150 nm in width. The separation between JJ1 and JJ2 is sufficiently shorter than the coherence length of aluminum (~1 μm). We note that the AMSs have been demonstrated in coupled JJs with the same separation (*32*). The junction length and width of the JJ1 and JJ2 are 100 and 600 nm, respectively. Furthermore, two larger JJs, named JJL1 and JJL2 with 2-μm width and 100-nm length, are prepared to form larger and smaller asymmetric SQUIDs. Subsequently, we place the gate electrodes on all the JJs to control them by the gate voltages. As depicted in Fig. 1C, we bias an electrical current I_1 when measuring the larger SQUID and measure the voltage difference V_1 as well. All the measurements were performed at 10 mK of the base temperature in our dilution refrigerator. In case of inducing the phase shift in JJ2 and JJL2, we added a bias current I_2 in the smaller SQUID.

RESULTS

First, we characterize the single JJ properties of JJ1 and JJ2 with the other JJs pinched off (see note S1 and fig. S1). The current-voltage relation (*I-V*) curve of JJ1 at an out-of-plane magnetic field $B = 0$ mT with $V_{g1} = -1.4$ V of the gate voltage for JJ1 with the other JJs pinched off is portrayed in Fig. 1D, wherein the supercurrent flows and the switching current of JJ1 is 0.2 μA. The switching

current of JJ1 is highly tunable as shown in Fig. 1E. The JJ2 indicates a similar switching current and the dependence on the gate voltage V_{g2} for JJ2 as shown in Fig. 1F.

As the first step, we evaluate the CPR of the single JJ1 by measuring V_1 and I_1 of the larger asymmetric SQUID with $V_{g1} = -1.4$ V, JJ2 off, $V_{gL1} = -1.4$ V, and JJL2 off. For the evaluation, V_1 as a function of I_1 and B are measured to obtain the switching current of the asymmetric SQUID. The asymmetric SQUID is used to evaluate the CPR because the switching current is approximately written as $I_{sc1}[\phi_{1c} + 2\pi\Phi_1(B)/\Phi_0] + I_{swL1}$ (*27*, *55*). Here, the single JJ1 CPR and the switching current of the single JJL1 are $I_{sc1}[\phi_{1c} + 2\pi\Phi_1(B)/\Phi_0]$ and I_{swL1}, respectively. ϕ_{1c} and $\Phi_0 = h/2e$ denote the constant phase difference decided by the critical current of JJL1 and the loop inductance and flux quantum, respectively. $\Phi_1(B)$ represents the magnetic flux in the larger loop, which depends on B and the loop area. Therefore, we subtract the background assigned to the Fraunhofer-type interference in JJL1 to obtain the single JJ1 CPR (see note S2 and fig. S2). Consequently, the single JJ1 CPR curve, $I_{sc1}[\phi_{1c} + 2\pi\Phi_1(B)/\Phi_0]$, is obtained as shown with black circles in Fig. 1G. We assume that the correction from the inductance and circulating supercurrent in the loop is ignorable, and the magnetic flux in the loops is linearly dependent on B (see note S4 and fig. S4). The CPR periodically oscillates, and its shape is skewed from the sinusoidal function of B, reflecting the short ballistic nature of JJ1. These results assure that our asymmetric SQUID can be used to evaluate the JJ1 CPR.

Then, the CPR of JJ1 coupled with JJ2 is studied with $(V_{g1}, V_{g2}) = (-1.4\text{ V}, -1.45\text{ V})$ and $(V_{gL1}, V_{gL2}) = (-1.4\text{ V}, -1.15\text{ V})$. These gate voltages produce similar switching currents of 0.2 μA in JJ1 and JJ2. For this sake, V_1 obtained as a function of I_1 and B is measured with JJL1 and JJL2 on. The coupled JJ1 CPR curve obtained by subtracting the same background data as the single JJ1 CPR evaluation is shown as green circles in Fig. 1G. The obtained CPR curve is highly modulated from that of JJ1 with no JJ2 and is not periodic. This modulation originates from the AMS formation in the coupled JJs, which makes the CPR of JJ1 dependent on ϕ_2. Now, B changes not only ϕ_1 but also ϕ_2 because both of the asymmetric SQUIDs are formed. Then, ϕ_2 is introduced as $2\pi\Phi_2(B)/\Phi_0$, where $\Phi_2(B)$ represents the magnetic flux in the smaller loop. As $|\Phi_2| < |\Phi_1|$ holds from the loop area relation, ϕ_1 and ϕ_2 evolve with B at the different ratios. Therefore, the $[\phi_1(B), \phi_2(B)]$ trace is depicted in Fig. 1H.

For instance, if B increases from $\Phi_1 = \Phi_2 = 0$, the trace of $(\phi_1, \phi_2) = [\phi_{1c} + 2\pi\Phi_1(B)/\Phi_0, 2\pi\Phi_2(B)/\Phi_0]$ moves with B from $(\phi_{1c}, 0)$ along the solid arrows in Fig. 1H. Reaching at $\phi_1 = \pi$, the trace is shifted to $\phi_1 = -\pi$ with the same ϕ_2 and moves along the solid arrow. The described solid lines correspond to the trace when ϕ_1 changes by $7 \times 2\pi$. We note that $-0.9\text{ mT} < B < 0.3\text{ mT}$ includes around seven periods in ϕ_1 seen in the single JJ1 CPR curve in Fig. 1G. Therefore, the green circles in Fig. 1G represent $I_{sc1}[\phi_{1c} + 2\pi\Phi_1(B)/\Phi_0, 2\pi\Phi_2(B)/\Phi_0]$, and the nonperiodic dependence on B indicates that the JJ1 CPR depends on ϕ_2 due to the AMS formation.

The trace lines do not fill the (ϕ_1, ϕ_2) plane in Fig. 1H. Therefore, only a portion of the two-dimensional CPR can be constructed from the green circles in Fig. 1G. A way to fill the entire (ϕ_1, ϕ_2) plane is to shift the trace lines along the vertical ϕ_2 axis and obtain the $[\phi_{1c} + 2\pi\Phi_1(B)/\Phi_0, 2\pi\Phi_2(B)/\Phi_0 + \Delta\phi_2]$ traces. Here, $\Delta\phi_2$ represents the shift of ϕ_2. For this sake, we add the bias current I_2 in the smaller SQUID because the finite supercurrent in the asymmetric SQUID shifts the phase differences of JJs following their CPRs and the SC loop inductance. To evaluate $\Delta\phi_2$ induced by I_2, we measure the JJ1

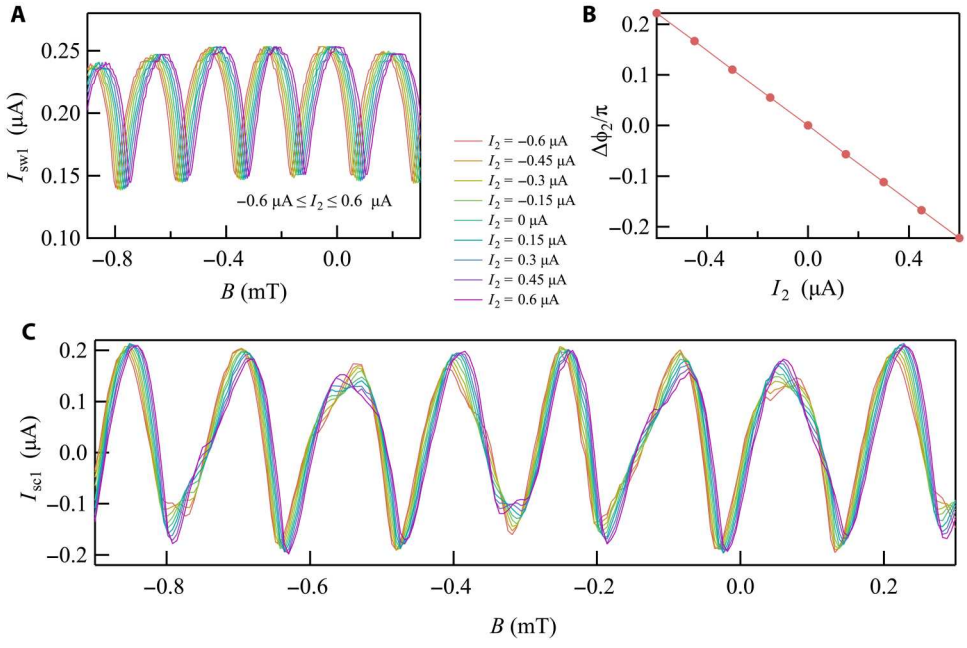

Fig. 2. Necessary dataset to obtain the two-dimensional CPR of JJ1 coupled to JJ2. (**A**) Switching current of JJ1 (I_{sw1}) as a function of B at $-0.6\text{ μA} \le I_2 \le 0.6\text{ μA}$ when JJ2 and JJL2 are on. The oscillation of switching current originates from the nonlocal Josephson effect derived from the coupling of JJ1 and JJ2. The curves shift along the B axis as I_2 varies, implying that the phase shift of JJ2 ($\Delta\phi_2$) is induced. (**B**) Evaluated $\Delta\phi_2$ as a function of I_2 from (A). $\Delta\phi_2$ is tunable with I_2 in the range of $-0.2\pi < \Delta\phi_2 < 0.2\pi$. (**C**) The obtained JJ1 supercurrent as a function of B at $-0.6\text{ μA} \le I_2 \le 0.6\text{ μA}$. Line colors specifying I_2 are consistent with those in (A). The curve shapes are modulated by changing I_2.

with (V_{g1}, V_{g2}) = (−1.4 V, −1.45 V), JJL1 off, and V_{gL2} = −1.15 V. Under this condition, the switching current of JJ1 (I_{sw1}) depends on ϕ_2 due to the nonlocal Josephson effect derived from the AMSs (*28*, *44*).

I_{sw1} is displayed in Fig. 2A as a function of B for several I_2 values between −600 and 600 nA. We note that I_2 in the range is smaller than the switching current of the smaller SDQUID. I_{sw1} oscillates with B, originating from the coherent coupling between JJ1 and JJ2. The oscillation pattern gradually shifts along the B axis as I_2 varied. This indicates that $\Delta\phi_2$ is induced by I_2, and the switching current is described as $I_{sw1}[2\pi\Phi_2(B)/\Phi_0 + \Delta\phi_2(I_2)]$. As the single oscillation period corresponds to 2π, $\Delta\phi_2(I_2)/2\pi$ is estimated from the $I_{sw1}[2\pi\Phi_2(B)/\Phi_0 + \Delta\phi_2(I_2)]$ curves as a ratio of the shift along the B axis from the curve of I_2 = 0 nA to the single oscillation period in B. The estimated $\Delta\phi_2$ versus I_2 is portrayed in Fig. 2B. In the range of −600 nA ≤ I_2 ≤ 600 nA, $\Delta\phi_2$ is tuned by ~0.4π.

Subsequently, we measure the CPR of JJ1 with JJ2 on by varying I_2. The CPR curves are presented as a function of B in Fig. 2C. The result for I_2 = 0 nA corresponds to the green data in Fig. 1G. The curve shape gradually varies with I_2, reflecting $I_{sc1}[\phi_{1c} + 2\pi\Phi_1(B)/\Phi_0, 2\pi\Phi_2(B)/\Phi_0 + \Delta\phi_2]$. Thus, we obtain the necessary CPR dataset to construct $I_{sc1}(\phi_1, \phi_2)$ in $-\pi \le \phi_1 \le \pi$ and $-\pi \le \phi_2 \le \pi$ (see note S3 and fig. S3). For clarity, we represent $I_{sc1}(\phi_1, \phi_2)$ in $-2\pi \le \phi_1 \le 2\pi$ and $-2\pi \le \phi_2 \le 2\pi$ in Fig. 3A by pasting several $I_{sc1}(\phi_1, \phi_2)$ data with ±2π shift along the ϕ_1 or ϕ_2 axes. The constructed CPR evidently depends on both ϕ_1 and ϕ_2 and looks point-symmetric to $\phi_1 = \phi_2 = 0$ as expected from the time-reversal relation of $I_{sc1}(\phi_1, \phi_2) = -I_{sc1}(-\phi_1, -\phi_2)$ for the coupled JJs. We note that Fig. 2C includes some effects from inductances of the SC loops and the possible ϕ_1 shift invoked by I_2, but we ignore them in our analysis to obtain Fig. 3A. This may cause the noise found in the two-dimensional CPR data in Fig. 3A (see note S4).

We numerically calculate the CPR of two coupled planar JJs. We use the tight-binding model to evaluate the energies of the ABSs formed in the coherently coupled JJs and calculate the supercurrent in JJ1 by the differential of the total energies by ϕ_1. The obtained numerical result is presented in Fig. 3B (see note S5 and fig. S5), which gives an excellent agreement with the experimental results. This agreement supports that the evaluated data exhibit the desired two-dimensional CPR of $I_{sc1}(\phi_1, \phi_2)$.

To discuss the φ junction, we focus on ϕ_1 yielding $I_{sc1}(\phi_1, \phi_2) = 0$ nA because no supercurrent flows in the ground state of the JJ. We plot ϕ_1 with $I_{sc1}(\phi_1, \phi_2) = 0$ nA as a function of ϕ_2 highlighted by a purple line in Fig. 3A . Here, we only indicate ϕ_1 continuously connecting to $\phi_1 = \phi_2 = 0$ and ignore the other $I_{sc1}(\phi_1, \phi_2) = 0$ nA around $\phi_1 = \pi$ because the system is time-reversal and spatial-inversion invariant at $\phi_2 = 0$, resulting in the ground state of JJ1 at $\phi_1 = 0$. The ground state gradually progresses along the purple line away from $\phi_1 = 0$ as ϕ_2 varies from $\phi_2 = 0$, indicating the φ junction of JJ1. The purple line oscillates with ϕ_2 period of 2π, which clearly proves that the φ junction originating from the AMSs can be tuned by a nonlocal phase difference.

To find the spontaneous supercurrent, i.e., the supercurrent in JJ1 with $\phi_1 = 0$, we plot line profiles of Fig. 3A at $\phi_2 = 0, \pm\pi/2$, and π in Fig. 3C. It is clear to see the curves at $\phi_2 = \pm\pi/2$ holding a finite supercurrent at $\phi_1 = 0$. This behavior is reproduced in line profiles of the numerical results in Fig. 3B at $\phi_2 = 0, \pm\pi/2$, and π as shown in Fig. 3D. We note that the maximum and minimum I_{sc1} of the CPR in Fig. 3 (C and D) depend on ϕ_2. This corresponds to I_{sw1} dependent on B, namely, ϕ_2 observed in Fig. 2A. Then, to confirm the gate tunability of the spontaneous supercurrent, we plot a line profile of Fig. 3A at $\phi_1 = 0$ in Fig. 3C, which represents $I_{sc1}(0, \phi_2)$. $I_{sc1}(0, \phi_2)$ oscillates as a function of ϕ_2. This means that the finite spontaneous supercurrent is controlled by the nonlocal phase difference. The spontaneous supercurrent as a function of ϕ_2 is approximately an odd function as expected from the time-reversal relation of $I_{sc1}(0, \phi_2) = -I_{sc1}(0, -\phi_2)$.

We note that the oscillation amplitude of the JJ1 CPR at $\phi_2 \simeq \pi$ (~0.1 μA) is smaller than that at $\phi_2 \simeq 0$ (~0.2 μA) as seen in Fig. 3 (A to D). The amplitude at $\phi_2 \simeq \pi$ is also smaller than that with JJ2 off (~0.2 μA) of the black circles in Fig. 1G. Therefore, when B makes $\phi_2 \simeq \pi$ (mod 2π), difference between the JJ1 supercurrent with JJ2 on and with JJ2 off becomes large. This is the reason why the discrepancy between I_{sc1} with JJ2 on and with JJ2 off in Fig. 1G becomes remarkable around −0.77, −0.56, −0.34, −0.14, and 0.084 mT. These B points correspond to $\phi_2 \simeq \pi$ (mod 2π) (see fig. S3C). Then, the phase shift of ϕ_2 induced by I_2 makes the remarkable modulation of the curves around the B points in Fig. 2C.

DISCUSSION

The observation of AJE means that the CPR of JJ1 is asymmetric to $\phi_1 = 0$ at $\phi_2 \neq 0, \pi$. The origin of the AJE or the asymmetric CPR has been associated with the AMS physics in the literature (*28*). To discuss the origin, we consider the ABS energies as a function of $\phi_1 \in [-\pi, \pi]$ in the single JJ1 and JJ2 with ϕ_2 fixed in [0, π]. With no coherent coupling, the ABS energies in the single JJ2 are constant with ϕ_1, while the ABS spectrum in JJ1 is symmetric with respect to $\phi_1 = 0$ and the energies monotonically decrease as ϕ_1 is swept away from $\phi_1 = 0$ (*25*). Then, the single ABS in JJ1 can cross the single ABS in JJ2 at two ϕ_1 points in [0, π] and [−π,0]. With the coherent coupling, the two ABSs are hybridized at the crossing points to open the energy gaps. At the crossing point in [0, π], elastic cotunneling hybridizes the ABSs while crossed Andreev reflection does at the point in [−π,0]. This difference induces the different energy gaps to cause the asymmetric Andreev spectrum to $\phi_1 = 0$ in the coupled JJ1 (see note S7 and fig. S7). I_{sc1} is derived from the differential of the ABS energies with ϕ_1. Consequently, the CPR of JJ1 becomes asymmetric to $\phi_1 = 0$, and the AJE can emerge.

The experimental and numerical results indicate that the oscillation amplitude of the JJ1 CPR at $\phi_2 \simeq \pi$ is smaller than that at $\phi_2 \simeq 0$ or that with no coherent coupling. Our additional calculation of the coupled JJs with the single conduction channel in each of JJs implies that the coupling energy of the JJ1 and JJ2 ABSs at $\phi_2 \simeq \pi$ is larger than that at $\phi_2 \simeq 0$. The larger coupling energy produces the larger modulation of the ABSs, resulting in the smaller I_{sc1} (see note S7 and fig. S7).

It may be valuable to refer to the SC diode effect in the coupled JJs (*45*, *47*, *48*). The SC diode effect is evaluated from comparison of the positive I_{sw1} with the negative I_{sw1} at fixed ϕ_2. This corresponds to compare the maximum I_{sc1} with the minimum I_{sc1} in the obtained CPR of JJ1 at the ϕ_2. Ideally, the SC diode effect could be obtained from the two-dimensional CPR in Fig. 3A by the comparison. However, because of the noise in the data originating from the inductance and the ϕ_1 shift by I_2 (see note S4), our CPR data do not have sufficient quality to reproduce the previously reported SC diode effect from the maximum and minimum I_{sc1} whose efficiency is typically small (~5%) (*45*).

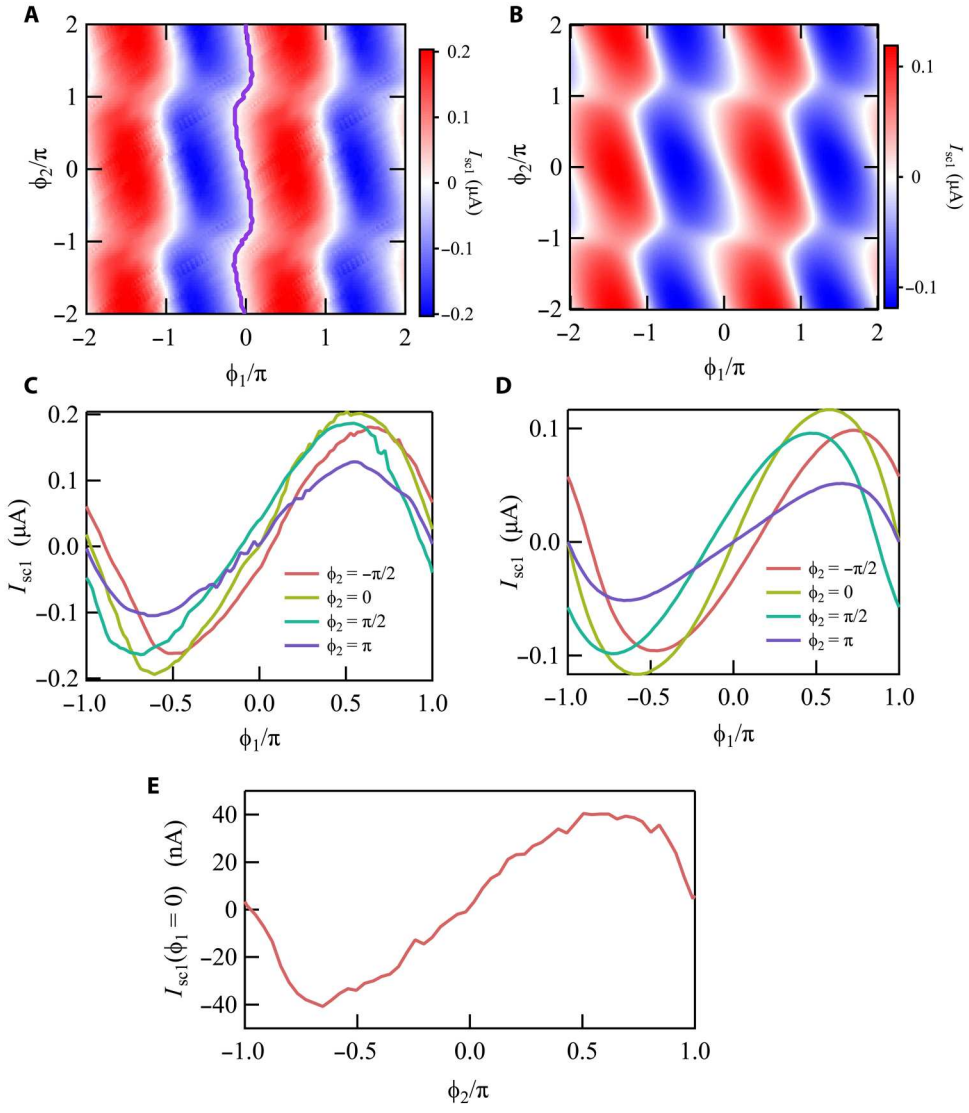

Fig. 3. The CPR of JJ1 coupled to JJ2 and the phase-tunable AJE. (**A**) The obtained two-dimensional CPR of JJ1 coupled to JJ2 is shown. The JJ1 supercurrent depends not only on ϕ_1 but also on ϕ_2, which means that the coherent coupling of JJ1 and JJ2 produces the nonlocal Josephson effect. A purple line on $I_{sc1}(\phi_1, \phi_2) = 0$ nA is extended from $(\phi_1, \phi_2) = (0,0)$, exhibiting the evolution of ϕ_1 for the ground state of JJ1 with ϕ_2. Therefore, $\phi_1 \neq 0$ on the purple line indicates that the ϕ junction is formed and tunable by ϕ_2. (**B**) Numerically calculated CPR of JJ1 coupled to JJ2 using the tight-binding model. This gives a good agreement with the experimental result in (A). (**C**) Line profiles at $\phi_1 = 0, \pm\pi/2, \pi$ in (A) are shown. (**D**) Line profiles at $\phi_1 = 0, \pm\pi/2, \pi$ in (B) are shown. (**E**) A line profile at $\phi_1 = 0$ in (A) is shown. The finite supercurrent flowing in JJ1 with $\phi_1 = 0$ and the spontaneous supercurrent is tunable with ϕ_2.

Last, we explore V_{g1} and V_{g2} dependence of the two-dimensional CPR of JJ1. The evaluated JJ1 CPRs with several (V_{g1}, V_{g2}) are summarized in Fig. 4 (see note S4 and fig. S4). For example, the panel at the top-left corner shows $I_{sc1}(\phi_1, \phi_2)$ at $(V_{g1}, V_{g2}) = (-1.4\ \text{V}, -1.95\ \text{V})$. The JJ1 CPR results at the same V_{g1} but different V_{g2} are exhibited in the same rows with the same color scales. Figure 4 indicates that the AJE behavior decreases as V_{g2} is made more negative, while the behavior is less modulated by V_{g1}. This gate dependence can be assigned to the relation of the numbers of ABSs in JJ1 and JJ2. In the case that the number of ABSs in JJ1 is smaller than that in JJ2, all the ABSs in JJ1 are coupled with the ABSs in JJ2. Therefore, the AJE behavior can remain evident. On the other hand, in the opposite case, some ABSs in JJ1 are not coupled with the ABSs in JJ2. Consequently, the AJE behavior becomes smaller as the number of ABSs in JJ2 decreases. This gate voltage dependence can be reproduced in our numerical calculation (see note S6 and fig. S6). Then, the gate dependence supports that the AJE in JJ1 emerges from the AMSs formed in the coupled JJs. We note that the AJE appears even in $V_{g1} = -1.7$ V where I_{sc1} is of the order of 10 nA. This means that the AJE behavior in JJ1 is not an artifact from our evaluation method in which we assume that Φ_1 and Φ_2 are linearly dependent on B and ignore the inductance term related to the circulating supercurrent in the SC loop because the small supercurrent makes the inductance effect smaller (see note S4 and fig. S4).

In our consideration, we do not include the spin-orbit interactions that the InAs quantum well holds. At least, the obtained AJE

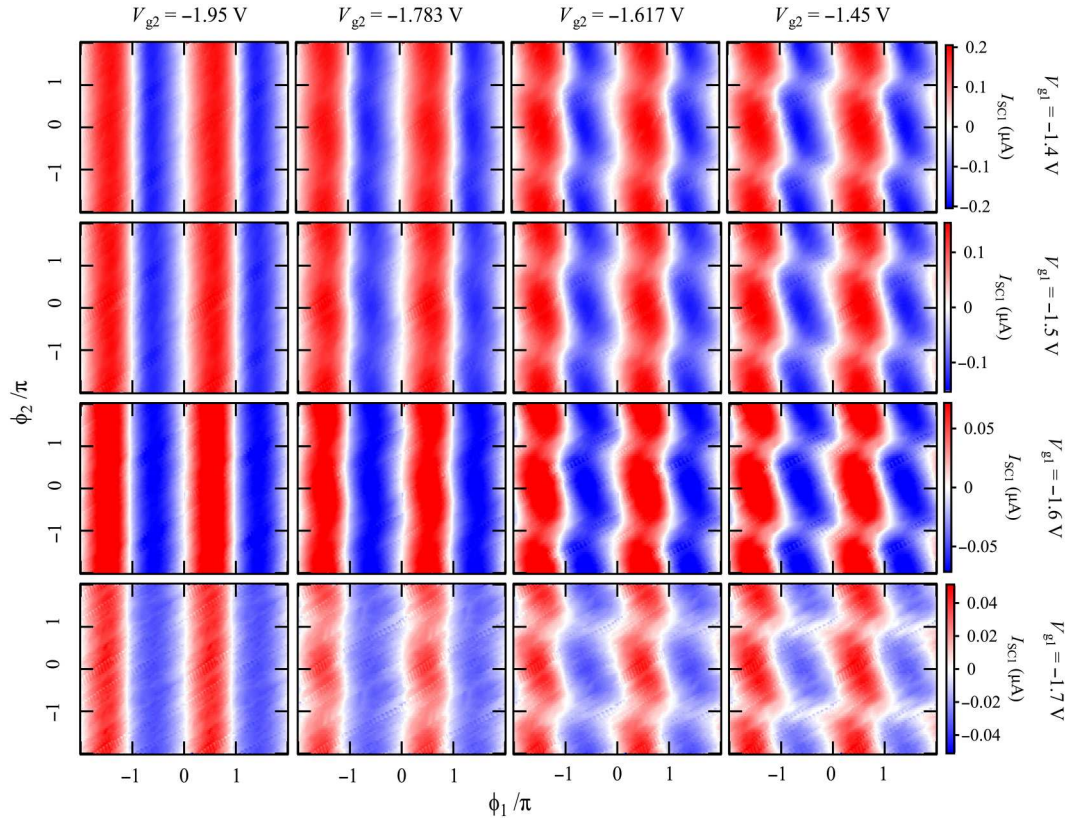

Fig. 4. Gate voltage dependence of the two-dimensional CPR of JJ1. The JJ1 CPR $I_{sc1}(\phi_1, \phi_2)$ results obtained at several sets of (V_{g1}, V_{g2}) are shown. The panels in the same row (column) are obtained at the same V_{g1} (V_{g2}), labeled on the right side (upside). In addition, the same row images are depicted with the same color scales placed on the right side. These results indicate that the dependence on ϕ_2 becomes weaker as V_{g2} becomes more negative while it is almost unchanged though V_{g1} is varied.

can be explained only by the coherent coupling, and it is difficult to discuss roles of the spin-orbit interactions in these results. To elucidate such physics, it may be useful to study the SC transport in the coupled JJs with the in-plane magnetic fields because the in-plane magnetic fields lifting the spin degeneracy produce the various SC phenomena related to the spin-orbit interactions in the single JJs such as the SC phase batteries, SC diodes, and Majorana zero modes.

In conclusion, we construct a two-dimensional CPR of a JJ coherently coupled to another JJ using asymmetric SQUIDs. From the CPR, we demonstrate the spontaneous supercurrent and ϕ junction controlled by the nonlocal phase difference, indicating the phase-tunable AJE. The obtained AJE contributes to the development of functional SC devices such as SC phase batteries and SC diodes. Our method for the two-dimensional CPR evaluation will be applicable to multiterminal JJs as well, where a single normal metal is coupled to several SC electrodes (*21*, *59*–*65*).

MATERIALS AND METHODS

Sample growth

The wafer structure has been grown via molecular beam epitaxy on a semi-insulating InP substrate. The stack materials from bottom to top are a 100-nm $In_{0.52}Al_{0.48}As$ buffer, a five-period 2.5-nm $In_{0.53}Ga_{0.47}As$/2.5 nm $In_{0.52}Al_{0.48}As$ superlattice, a 1-μm-thick metamorphic graded buffer stepped from $In_{0.52}Al_{0.48}As$ to $In_{0.84}Al_{0.16}As$, a 33-nm graded $In_{0.84}Al_{0.16}As$ to $In_{0.81}Al_{0.19}As$ layer, a 25-nm $In_{0.81}Al_{0.19}As$ layer, a 4-nm $In_{0.81}Ga_{0.19}As$ lower barrier, a 5-nm InAs quantum well, a 10-nm $In_{0.81}Ga_{0.19}As$ top barrier, two monolayers of GaAs, and lastly, an 8.7-nm layer of epitaxial Al. The top Al layer has been grown in the same chamber without breaking the vacuum. The two-dimensional electron gas (2DEG) accumulates in the InAs quantum well.

Device fabrication

In this study, conventional electron beam lithography was used to fabricate JJs. We etched out the aluminum film using the type D etchant after we defined the mesa of the InAs quantum well with 1:1:8 of H_3PO_4:H_2O_2:H_2O etchant. Subsequently, we grew a 30-nm-thick Al_2O_3 film by atomic layer deposition and deposited Ti and Au to make the gate electrodes.

Measurement

For the measurement of the switching current, we measured the *I*-*V* curves of JJ1 for various conditions. When switching JJL1 or JJL2 off to measure the single or coupled JJ1, we set $V_{gL1} \leq -1.9$ V or $V_{gL2} \leq -2.0$ V. When switching JJL1 or JJL2 on to form the asymmetric SQUIDs, we set $V_{gL1} = -1.4$ V or $V_{gL2} = -1.15$ V. The switching currents of JJL1 and JJL2 at $V_{gL1} = -1.4$ V and $V_{gL2} = -1.15$ V are 0.8 and 1.0 μA, respectively. When pinching off JJL1 and JJL2, we set V_{gL1} (V_{gL2}) = −4 V.

Supplementary Materials

This PDF file includes:

Notes S1 to S7
Figs. S1 to S7

REFERENCES AND NOTES

1. C. Baumgartner, L. Fuchs, A. Costa, S. Reinhardt, S. Gronin, G. C. Gardner, T. Lindemann, M. J. Manfra, P. E. Faria Junior, D. Kochan, J. Fabian, N. Paradiso, C. Strunk, Supercurrent rectification and magnetochiral effects in symmetric Josephson junctions. *Nat. Nanotechnol.* **17**, 39–44 (2022).
2. R. Wakatsuki, Y. Saito, S. Hoshino, Y. M. Itahashi, T. Ideue, M. Ezawa, Y. Iwasa, N. Nagaosa, Nonreciprocal charge transport in noncentrosymmetric superconductors. *Sci. Adv.* **3**, e1602390 (2017).
3. F. Ando, Y. Miyasaka, T. Li, J. Ishizuka, T. Arakawa, Y. Shiota, T. Moriyama, Y. Yanase, T. Ono, Observation of superconducting diode effect. *Nature* **584**, 373–376 (2020).
4. R. M. Lutchyn, E. P. A. M. Bakkers, L. P. Kouwenhoven, P. Krogstrup, C. M. Marcus, Y. Oreg, Majorana zero modes in superconductor–semiconductor heterostructures. *Nature Reviews Materials* **3**, 52–68 (2018).
5. B. D. Josephson, Possible new effects in superconductive tunnelling. *Phys. Letters* **1**, 251–253 (1962).
6. A. Buzdin, A. E. Koshelev, Periodic alternating 0- and π-junction structures as realization of φ-Josephson junctions. *Physical Review B* **67**, 220504 (2003).
7. A. Buzdin, Direct coupling between magnetism and superconducting current in Josephson phi junction. *Phys. Rev. Lett.* **101**, 107005 (2008).
8. Y. Tanaka, T. Yokoyama, N. Nagaosa, Manipulation of the Majorana fermion, Andreev reflection, and Josephson current on topological insulators. *Phys. Rev. Lett.* **103**, 107002 (2009).
9. A. Zazunov, R. Egger, T. Jonckheere, T. Martin, Anomalous Josephson current through a spin-orbit coupled quantum dot. *Phys. Rev. Lett.* **103**, 147004 (2009).
10. T. Yokoyama, M. Eto, Y. V. Nazarov, Anomalous Josephson effect induced by spin-orbit interaction and Zeeman effect in semiconductor nanowires. *Physical Review B* **89**, 195407 (2014).
11. E. Strambini, A. Iorio, O. Durante, R. Citro, C. Sanz-Fernández, C. Guarcello, I. V. Tokatly, A. Braggio, M. Rocci, N. Ligato, V. Zannier, L. Sorba, F. S. Bergeret, F. Giazotto, A Josephson phase battery. *Nature Nanotechnology* **15**, 656–660 (2020).
12. D. B. Szombati, S. Nadj-Perge, D. Car, S. R. Plissard, E. P. A. M. Bakkers, L. P. Kouwenhoven, Josephson ϕ_0-junction in nanowire quantum dots. *Nat. Phys.* **12**, 568–572 (2016).
13. W. Mayer, M. C. Dartiailh, J. Yuan, K. S. Wickramasinghe, E. Rossi, J. Shabani, Gate controlled anomalous phase shift in Al/InAs Josephson junctions. *Nat. Commun.* **11**, 212 (2020).
14. A. Assouline, C. Feuillet-Palma, N. Bergeal, T. Zhang, A. Mottaghizadeh, A. Zimmers, E. Lhuillier, M. Eddrie, P. Atkinson, M. Aprili, H. Aubin, Spin-orbit induced phase-shift in Bi_2Se_3 Josephson junctions. *Nat. Commun.* **10**, 126 (2019).
15. S. Pal, C. Benjamin, Quantized Josephson phase battery. *EPL (Europhysics Letters)* **126**, 57002 (2019).
16. H. Sickinger, A. Lipman, M. Weides, R. G. Mints, H. Kohlstedt, D. Koelle, R. Kleiner, E. Goldobin, Experimental evidence of a φ Josephson junction. *Phys. Rev. Lett.* **109**, 107002 (2012).
17. R. Menditto, H. Sickinger, M. Weides, H. Kohlstedt, D. Koelle, R. Kleiner, E. Goldobin, Tunable φ Josephson junction ratchet. *Physical Review E* **94**, 042202 (2016).
18. B. Turini, S. Salimian, M. Carrega, A. Iorio, E. Strambini, F. Giazotto, V. Zannier, L. Sorba, S. Heun, Josephson diode effect in high-mobility InSb nanoflags. *Nano Lett.* **22**, 8502–8508 (2022).
19. B. Pal, A. Chakraborty, P. K. Sivakumar, M. Davydova, A. K. Gopi, A. K. Pandeya, J. A. Krieger, Y. Zhang, M. Date, S. Ju, N. Yuan, N. B. M. Schröter, L. Fu, S. S. P. Parkin, Josephson diode effect from Cooper pair momentum in a topological semimetal. *Nat. Phys.* **18**, 1228–1233 (2022).
20. R. S. Souto, M. Leijnse, C. Schrade, Josephson diode effect in supercurrent interferometers. *Phys. Rev. Lett.* **129**, 267702 (2022).
21. M. Gupta, G. V. Graziano, M. Pendharkar, J. T. Dong, C. P. Dempsey, C. Palmstrøm, V. S. Pribiag, Gate-tunable superconducting diode effect in a three-terminal Josephson device. *Nat. Commun.* **14**, 3078 (2023).
22. C. Ciaccia, R. Haller, A. C. C. Drachmann, T. Lindemann, M. J. Manfra, C. Schrade, C. Schönenberger, Gate-tunable Josephson diode in proximitized inas supercurrent interferometers. *Phys. Rev. Research* **5**, 033131 (2023).
23. M. Valentini, O. Sagi, L. Baghumyan, T. de Gijsel, J. Jung, S. Calcaterra, A. Ballabio, J. A. Servin, K. Aggarwal, M. Janik, T. Adletzberger, R. S. Souto, M. Leijnse, J. Danon, C. Schrade, E. Bakkers, D. Chrastina, G. Isella, G. Katsaros, Radio frequency driven superconducting diode and parity conserving Cooper pair transport in a two-dimensional germanium hole gas. arXiv:2306.07109 (2023). http://arxiv.org/abs/2306.07109.
24. A. Furusaki, M. Tsukada, Current-carrying states in Josephson junctions. *Physical Review B* **43**, 10164–10169 (1991).
25. C. W. J. Beenakker, H. van Houten, Josephson current through a superconducting quantum point contact shorter than the coherence length. *Phys. Rev. Lett.* **66**, 3056–3059 (1991).
26. J.-D. Pillet, C. H. L. Quay, P. Morfin, C. Bena, A. L. Yeyati, P. Joyez, Andreev bound states in supercurrent-carrying carbon nanotubes revealed. *Nature Phys.* **6**, 965–969 (2010).
27. F. Nichele, E. Portolés, A. Fornieri, A. . M. Whiticar, A. . C. . C. Drachmann, S. Gronin, T. Wang, G. . C. Gardner, C. Thomas, A. . T. Hatke, M. . J. Manfra, C. . M. Marcus, Relating Andreev bound states and supercurrents in hybrid Josephson junctions. *Phys. Rev. Lett.* **124**, 226801 (2020).
28. J.-D. Pillet, V. Benzoni, J. Griesmar, J.-L. Smirr, Ç. O. Girit, Nonlocal Josephson effect in Andreev molecules. *Nano Lett.* **19**, 7138–7143 (2019).
29. V. Kornich, H. S. Barakov, Y. V. Nazarov, Overlapping Andreev states in semiconducting nanowires: Competition of one-dimensional and three-dimensional propagation. *Physical Review B* **101**, 195430 (2020).
30. O. Kürtössy, Z. Scherübl, G. Fülöp, I. E. Lukács, T. Kanne, J. Nygård, P. Makk, S. Csonka, Andreev molecule in parallel InAs nanowires. *Nano Lett.* **21**, 7929–7937 (2021).
31. Z. Su, A. B. Tacla, M. Hocevar, D. Car, S. R. Plissard, E. P. A. M. Bakkers, A. J. Daley, D. Pekker, S. M. Frolov, Andreev molecules in semiconductor nanowire double quantum dots. *Nat. Commun.* **8**, 585 (2017).
32. S. Matsuo, T. Imoto, T. Yokoyama, Y. Sato, T. Lindemann, S. Gronin, G. C. Gardner, S. Nakosai, Y. Tanaka, M. J. Manfra, S. Tarucha, Phase-dependent Andreev molecules and superconducting gap closing in coherently coupled Josephson junctions. arXiv:2303.10540 (2023). http://arxiv.org/abs/2303.10540.
33. M. Coraiola, D. Z. Haxell, D. Sabonis, H. Weisbrich, A. E. Svetogorov, M. Hinderling, S. C. ten Kate, E. Cheah, F. Krizek, R. Schott, W. Wegscheider, J. C. Cuevas, W. Belzig, F. Nichele, Hybridisation of Andreev bound states in three-terminal Josephson junctions. arXiv:2302.14535 (2023). http://arxiv.org/abs/2302.14535.
34. V. Kornich, H. S. Barakov, Y. V. Nazarov, Fine energy splitting of overlapping Andreev bound states in multiterminal superconducting nanostructures. *Physical Review Research* **1**, 033004 (2019).
35. P. Recher, E. V. Sukhorukov, D. Loss, Andreev tunneling, Coulomb blockade, and resonant transport of nonlocal spin-entangled electrons. *Phys. Rev. B* **63**, 165314 (2001).
36. G. B. Lesovik, T. Martin, G. Blatter, Electronic entanglement in the vicinity of a superconductor. *The European Physical Journal B - Condensed Matter and Complex Systems* **24**, 287–290 (2001).
37. P. Recher, D. Loss, Superconductor coupled to two Luttinger liquids as an entangler for electron spins. *Phys. Rev. B* **65**, 165327 (2002).
38. C. Bena, S. Vishveshwara, L. Balents, M. P. A. Fisher, Quantum entanglement in carbon nanotubes. *Phys. Rev. Lett.* **89**, 037901 (2002).
39. N. M. Chtchelkatchev, G. Blatter, G. B. Lesovik, T. Martin, Bell inequalities and entanglement in solid-state devices. *Phys. Rev. B* **66**, 161320 (2002).
40. L. Hofstetter, S. Csonka, J. Nygard, C. Schonenberger, Cooper pair splitter realized in a two-quantum-dot Y-junction. *Nature* **461**, 960–963 (2009).
41. L. G. Herrmann, F. Portier, P. Roche, A. L. Yeyati, T. Kontos, C. Strunk, Carbon nanotubes as Cooper-pair beam splitters. *Phys. Rev. Lett.* **104**, 026801 (2010).
42. S. Baba, C. Junger, S. Matsuo, A. Baumgartner, Y. Sato, H. Kamata, K. Li, S. Jeppesen, L. Samuelson, H. Q. Xu, C. Schonenberger, S. Tarucha, Cooper-pair splitting in two parallel InAs nanowires. *New J. Phys.* **20**, 063021 (2018).
43. K. Ueda, S. Matsuo, H. Kamata, S. Baba, Y. Sato, Y. Takeshige, K. Li, S. Jeppesen, L. Samuelson, H. Xu, S. Tarucha, Dominant nonlocal superconducting proximity effect due to electron-electron interaction in a ballistic double nanowire. *Advances* **5**, (2019).
44. S. Matsuo, J. S. Lee, C.-Y. Chang, Y. Sato, K. Ueda, C. J. Palmstrøm, S. Tarucha, Observation of nonlocal Josephson effect on double InAs nanowires. *Commun Phys* **5**, 221 (2022).
45. S. Matsuo, T. Imoto, T. Yokoyama, Y. Sato, T. Lindemann, S. Gronin, G. C. Gardner, M. J. Manfra, S. Tarucha, Josephson diode effect derived from short-range coherent coupling. *Nat. Phys.* **19**, 1636–1641 (2023).
46. D. Z. Haxell, M. Coraiola, M. Hinderling, S. C. Ten Kate, D. Sabonis, A. E. Svetogorov, W. Belzig, E. Cheah, F. Krizek, R. Schott, W. Wegscheider, F. Nichele, Demonstration of the nonlocal Josephson effect in Andreev molecules. *Nano Lett.* **23**, 7532–7538 (2023).
47. J.-D. Pillet, S. Annabi, A. Peugeot, H. Riechert, E. Arrighi, J. Griesmar, L. Bretheau, Josephson diode effect in Andreev molecules. *Phys. Rev. Research* **5**, 033199 (2023).
48. E. W. Hodt, J. Linder, On-off switch and sign change for a nonlocal Josephson diode in spin-valve Andreev molecules. *Phys. Rev. B* **108**, 174502 (2023).
49. M. Kocsis, Z. Scherübl, G. Fülöp, P. Makk, S. Csonka, Strong nonlocal tuning of the current-phase relation of a quantum dot based Andreev molecule. arXiv:2303.14842 (2023). http://arxiv.org/abs/2303.14842.

50. F. Pientka, A. Keselman, E. Berg, A. Yacoby, A. Stern, B. I. Halperin, Topological superconductivity in a planar Josephson junction. *Phys Rev. X* **7**, 021032 (2017).
51. H. Ren, F. Pientka, S. Hart, A. T. Pierce, M. Kosowsky, L. Lunczer, R. Schlereth, B. Scharf, E. M. Hankiewicz, L. W. Molenkamp, B. I. Halperin, A. Yacoby, Topological superconductivity in a phase-controlled Josephson junction. *Nature* **569**, 93–98 (2019).
52. A. Fornieri, A. M. Whiticar, F. Setiawan, E. Portolés, A. C. C. Drachmann, A. Keselman, S. Gronin, C. Thomas, T. Wang, R. Kallaher, G. C. Gardner, E. Berg, M. J. Manfra, A. Stern, C. M. Marcus, F. Nichele, Evidence of topological superconductivity in planar Josephson junctions. *Nature* **569**, 89–92 (2019).
53. O. Lesser, Y. Oreg, A. Stern, One-dimensional topological superconductivity based entirely on phase control. *Phys. Rev. B* **106**, L241405 (2022).
54. M. Luethi, H. F. Legg, K. Laubscher, D. Loss, J. Klinovaja, Majorana bound states in germanium Josephson junctions via phase control. arXiv:2304.12689 (2023). http://arxiv.org/abs/2304.12689.
55. M. L. D. Rocca, M. Chauvin, B. Huard, H. Pothier, D. Esteve, C. Urbina, Measurement of the current-phase relation of superconducting atomic contacts. *Phys. Rev. Lett.* **99**, 127005 (2007).
56. J. Shabani, M. Kjaergaard, H. J. Suominen, Y. Kim, F. Nichele, K. Pakrouski, T. Stankevic, R. M. Lutchyn, P. Krogstrup, R. Feidenhans'l, S. Kraemer, C. Nayak, M. Troyer, C. M. Marcus, C. J. Palmstrøm, Two-dimensional epitaxial superconductor-semiconductor heterostructures: A platform for topological superconducting networks. *Phys. Rev. B* **93**, 155402 (2016).
57. M. Kjaergaard, F. Nichele, H. J. Suominen, M. P. Nowak, M. Wimmer, A. R. Akhmerov, J. A. Folk, K. Flensberg, J. Shabani, C. J. Palmstrom, C. M. Marcus, Quantized conductance doubling and hard gap in a two-dimensional semiconductor-superconductor heterostructure. *Nat. Commun.* **7**, 12841 (2016).
58. M. Kjaergaard, H. J. Suominen, M. P. Nowak, A. R. Akhmerov, J. Shabani, C. J. Palmstrøm, F. Nichele, C. M. Marcus, Transparent semiconductor-superconductor interface and induced gap in an epitaxial heterostructure Josephson junction. *Phys. Rev. Applied* **7**, 034029 (2017).
59. A. Freyn, B. Douçot, D. Feinberg, R. Mélin, Production of nonlocal quartets and phase-sensitive entanglement in a superconducting beam splitter. *Phys. Rev. Lett.* **106**, 257005 (2011).
60. A. W. Draelos, M.-T. Wei, A. Seredinski, H. Li, Y. Mehta, K. Watanabe, T. Taniguchi, I. V. Borzenets, F. Amet, G. Finkelstein, Supercurrent flow in multiterminal graphene Josephson junctions. *Nano Lett.* **19**, 1039–1043 (2019).
61. N. Pankratova, H. Lee, R. Kuzmin, K. Wickramasinghe, W. Mayer, J. Yuan, M. G. Vavilov, J. Shabani, V. E. Manucharyan, Multiterminal Josephson effect. *Phys. Rev. X* **10**, 031051 (2020).
62. G. V. Graziano, J. S. Lee, M. Pendharkar, C. J. Palmstrøm, V. S. Pribiag, Transport studies in a gate-tunable three-terminal Josephson junction. *Physical Review B* **101**, 054510 (2020).
63. A. H. Pfeffer, J. E. Duvauchelle, H. Courtois, R. Mélin, D. Feinberg, F. Lefloch, Subgap structure in the conductance of a three-terminal Josephson junction. *Phys. Rev. B* **90**, 075401 (2014).
64. Y. Cohen, Y. Ronen, J.-H. Kang, M. Heiblum, D. Feinberg, R. Mélin, H. Shtrikman, Nonlocal supercurrent of quartets in a three-terminal Josephson junction. *Proc. Natl. Acad. Sci.* **115**, 6991–6994 (2018).
65. E. Strambini, S. D. Ambrosio, F. Vischi, F. S. Bergeret, Y. V. Nazarov, F. Giazotto, The ω-SQUIPT as a tool to phase-engineer Josephson topological materials. *Nat. Nanotechnol.* **11**, 1055–1059 (2016).

Acknowledgments: We thank S. Kawabata for the discussion. **Funding:** This work was supported by JSPS Grant-in-Aid for Scientific Research (S) (grant no. JP19H05610), JST PRESTO (grant no. JPMJPR18L8), JST FOREST (grant no. JPMJFR223A), JSPS Grant-in-Aid for Early-Career Scientists (grant no. 18 K13484), and Advanced Technology Institute Research Grants. **Author contributions:** S.M. conceived the experiments. T.L., S.G., G.C.G., and M.J.M. grew wafers to form InAs 2DEG quantum wells covered with epitaxial aluminum. S.M. fabricated the devices. S. M. and T.I. performed measurements. S.M., T.I., Y.S., and S.T. analyzed the data. T.Y. performed numerical calculations. S.T. supervised the study. **Competing interests:** The authors declare that they have no competing interests. **Data and materials availability:** All data needed to evaluate the conclusions in the paper are present in the paper and/or the Supplementary Materials. The data that support the findings of this study are available from the Zenodo repository at https://doi.org/10.5281/zenodo.10036295.

Submitted 22 June 2023
Accepted 14 November 2023
Published 13 December 2023
10.1126/sciadv.adj3698